Implementation of a diffuse interface method in an LES solver

Milan Pelletier, Davy Nayigizente, Schmitt Thomas, Sébastien Ducruix

Noname manuscript No.
(will be inserted by the editor)

Implementation of a diffuse interface method in an LES solver

Milan Pelletier · Davy Nayigizente · Thomas Schmitt · Sébastien Ducruix

the date of receipt and acceptance should be inserted later

Abstract This study introduces a compressible diffuse interface method to treat flow dynamics for regimes ranging from subcritical two-phase flows to supercritical flows. The model relies on a cubic equation of state to take advantage of its wide domain of validity. This choice requires a careful treatment in areas where the fluid state lies in the binodal region. In this case, thermodynamic equilibrium is computed, yielding a two-phase stable fluid state. The model can be related to the family of multifluid methods such as Baer and Nunziato's 7-equation model (1986), considering speed, mechanical, thermal and thermodynamic relaxations. The model is integrated in the AVBP solver, jointly developed by CERFACS and IFPEN. This paper details the modified thermodynamics and derivation of the consistent boundary conditions and numerical schemes. Numerical validations are finally provided.

Keywords Real Gas · Transcritical flows · Two-phase flows · Diffuse Interface Model · Homogeneous Equilibrium Method · Hyperbolic Systems

1 Introduction

Many propulsion devices, such as liquid rocket engines (during ignition), Diesel engines (during compression) or aeronautical engines operate over a wide range of chamber pressure. As a consequence, they are likely to involve thermodynamic states that can range from subcritical to supercritical conditions. In particular, transition from one regime to the other is encountered. The question of supercritical flows in combustion chambers has been and still is widely studied [2,10,13,28]. Such flows require a description of the non-idealities in the molecular interactions, adressed by the Real-Gas (RG) thermodynamics. Among RG closures, cubic Equations of States (EoS), such as Van der Waals [27], Peng-Robinson [16] or Soave Redlich Kwong [24], have been deeply studied and prove to be relevant for supercritical simulations [7, 14, 22, 25, 26]. However, in the subcritical domain, phase transitions occur and models are needed to handle both liquid-gas interfaces and atomization. Interface models can be split in two classes: Sharp Interface Models (e.g. Level-Set Method [5, 15]), representing the interface as a discontinuity and Diffuse Interface Models (e.g. Multifluid Methods [1, 8, 17]), for which the interface takes a diffuse form. In the following, a diffuse interface approach is chosen as it offers a convenient framework for multispecies compressible flows on unstructured grids. Also, as the interface is not explicitely tracked, the extension from subcritical two-phase flows to supercritical flows is expected to be more natural. The challenge here is then to blend the subcritical diffuse interface model with the supercritical-adapted cubic EoS to provide a description of the flow in the whole range of thermodynamic states encountered in industrial devices.

The objective of this work is to extend the use of cubic EoS to the subcritical regime. This is done by computing Homogeneous Equilibrium in the binodal region. This paper describes the extended thermodynamics in detail and its integration in a compressible solver.

M. Pelletier
E-mail: milan.pelletier@centralesupelec.fr
D. Nayigizente
E-mail: davy.nayigizente@centralesupelec.fr
T. Schmitt
E-mail: thomas.schmitt@centralesupelec.fr
S. Ducruix
E-mail: sebastien.ducruix@centralesupelec.fr
Laboratoire EM2C, CNRS, CentraleSupélec, Université Paris-Saclay, 3, rue Joliot Curie, 91192 Gif-sur-Yvette cedex, France

The present paper is structured as follows: section 2 presents the flow model and the thermodynamic closure. In section 3, the derivation of important thermo-mechanical quantities will be presented, that allow the use of Taylor-Galerkin [4] numerical methods and Navier-Stokes Characteristic Boundary Conditions. Eventually, in section 4, one-dimensional and two-dimensional test cases are detailed to validate theoretical developments and implementation of the method.

2 Flow Model

2.1 System of Equations

The flow model is based on classical Euler equations. For the sake of conciseness, the developments are presented using a one-dimensional formulation, as they can be extended to multiple dimensions without difficulty (tridimensional developments are given in appendix B. The partial differential equation writes:

$$\frac{\partial U}{\partial t} + \frac{\partial \mathscr{F}(U)}{\partial x} = 0, \tag{1}$$

where U and $\mathscr{F}(U)$ represent respectively the vector of conserved variables and their fluxes, given by:

$$U = \begin{pmatrix} \rho \\ \rho u \\ \rho e_{\text{tot}} \end{pmatrix} \quad \text{and} \quad \mathscr{F}(U) = \begin{pmatrix} \rho u \\ \rho u^2 + P \\ (\rho e_{\text{tot}} + P)u \end{pmatrix}. \tag{2}$$

The usual notations are used here, with ρ the density, u the velocity, P the pressure and total specific energy $e_{\text{tot}} = e_s + e_c$, e_s being the sensible energy and indicating the kinetic energy $e_c = \frac{u^2}{2}$. This system of equations must be closed by an EoS.

2.2 Thermodynamic Closure

Among the possible choices, cubic EoS have proven to be a good trade-off between simplicity, accuracy and ability to handle phase change for multispecies mixtures [19, 28]. In the monospecies case, such EoS writes:

$$P = \frac{\rho r T}{1 - \rho b_{\text{EoS}}} - \frac{a_{\text{EoS}}(T)\rho^2}{1 + \varepsilon_1 \rho + \varepsilon_2 \rho^2}, \tag{3}$$

with T the temperature, a_{EoS} and b_{EoS} the EoS coefficients, $r = \frac{R}{W}$, R being the perfect gas constant and W the species molar mass and $(\varepsilon_1, \varepsilon_2)$ the EoS parameters. The present work is based on Soave-Redlich-Kwong EoS [24], which corresponds to $\varepsilon_1 = b$ and $\varepsilon_2 = 0$.

Although cubic EoS closures guarantee the strict hyperbolicity of Euler's equations in supercritical and transcritical regimes, this is not always verified in subcritical regimes. More precisely, in the spinodal region, the speed of sound becomes imaginary, as it appears in Figure 1a. This is actually a consequence of the instability of the fluid in this thermodynamic region.

In the case where the thermodynamic state lies in the binodal region, the strategy used here is to consider phase separation of the unstable fluid following the Homogeneous Equilibrium Method, as it is done for example in [3] with the Stiffened-Gas EoS [9]. This thermodynamic closure consists in considering that the fluid is at mechanical, thermal and thermodynamic equilibrium at all time. More precisely, it corresponds to taking into account the phase change whenever the fluid state (ρ, e_s) is within the binodal region (see Figure 1b). In this case, as the one-phase fluid state is either metastable or unstable, the two-phase stable mixture is computed so that both phase have the same temperature, pressure and Gibbs free energy g, that is:

$$P_\ell = P_v = P, \tag{4}$$

$$T_\ell = T_v = T, \tag{5}$$

$$g_\ell = g_v = g, \tag{6}$$

respecting mixture density and specific sensible energy. Subscripts ℓ and v indicate respectively the liquid and vapour phases.

At this point, it is interesting to mention that this flow model together with the Homogeneous Equilibrium thermodynamic closure for subcritical points, can be related to the family of multifluid models derived from Baer and Nunziato's seven-equation model [1]. This model represents two phase flows by allowing vapour and liquid

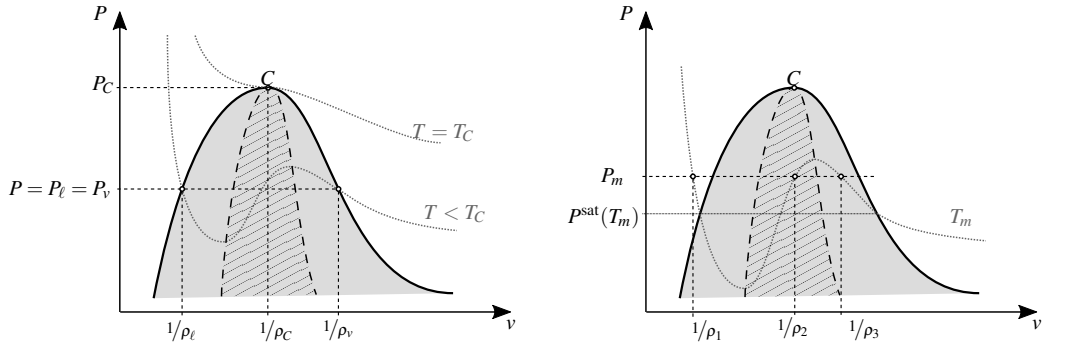

(a) Grey area represents the *binodal region*, delimited by the saturation curve. C indicates the critical point. Hatched area shows the *spinodal region*, where isotherms (dotted lines) have a positive slope. In this area, the speed of sound may become imaginary.

(b) Solutions of the cubic EoS are shown for a given couple (P_m, T_m). In this case, the stable solution, ρ_1 is pure liquid. ρ_2 is unstable as it lies in the spinodal region. ρ_3 is in the binodal region, hence the metastability of this solution

Fig. 1: Clapeyron diagrams for a cubic EoS.

phases to take different velocities, temperatures and chemical potentials, bound together by relaxation terms. Various models have then been derived from this one by considering infinitely fast relaxation of either one [20], two [8, 12] or all of these parameters [3, 6].

The model studied here then corresponds to Baer and Nunziato's with homogeneous equilibrium. The most common models of this form found in the literature use different EoS to describe the thermodynamics of each phase. This may allow more accurate behaviour in the pure phases, especially in the lower pressure domain. Yet, it would require a specific treatment to extend this representation to the supercritical and stable-single-phase domains, where the fluid stable state no longer consists in an equilibrium of two separate phases. This is the main reason why this methodology is considered here.

2.3 Practical implementation

Let ρ^p and e_s^p be the density and energy predicted by the numerical scheme. In the first place, the *one-phase* temperature T_m is determined finding the zero of function θ defined by:

$$\theta(\rho^p, T) = \frac{e_s^p - e_s^{\text{EoS}}(\rho^p, T)}{e_s^p}, \tag{7}$$

where e_s^{EoS} is the sensible energy computed from the EoS.

Once this temperature is obtained, *one-phase* pressure is computed as $P_m = P^{\text{EoS}}(\rho^p, T_m)$. The densities that satisfy the cubic EoS for the obtained (P_m, T_m) are computed from the EoS. If multiple roots are found, their fugacity is compared. The minimal fugacity solution being the stable one, the flow state is kept as single-phase if the predicted density is the one of minimal fugacity. Otherwise, a two-phase equilibrium must be computed.

To achieve this, the algorithm consists in cancelling the fugacities imbalance between both phases. First, one can introduce the two-phase mixture definitions:

$$\begin{cases} \rho = \alpha_\ell \rho_\ell + (1-\alpha_\ell)\rho_v & \text{(8a)} \\ \rho e_s = \alpha_\ell \rho_\ell e_{s,\ell} + (1-\alpha_\ell)\rho_v e_{s,v}, & \text{(8b)} \end{cases}$$

where α_ℓ represents the liquid volume fraction. These expressions can lead to two formulations of the volume fraction, which are equivalent at equilibrium:

$$\begin{cases} \alpha_{\ell,\rho} = \dfrac{\rho - \rho_v}{\rho_\ell - \rho_v} & \text{(9a)} \\ \alpha_{\ell,e} = \dfrac{\rho e_s - \rho_v e_{s,v}}{\rho_\ell e_{s,\ell} - \rho_v e_{s,v}}. & \text{(9b)} \end{cases}$$

It is convenient to introduce, for each phase $k \in \{\ell, v\}$ the quantity F_k defined from the fugacity f_k as:

$$F_k = \ln(f_k). \tag{10}$$

For a given set of values $(T^i, P^i, \rho_\ell^i, \rho_v^i, e_{s,\ell}^i, e_{s,v}^i)$, supposedly not at equilibrium, one can compute the corresponding $(\alpha_{\ell,\rho}, \alpha_{\ell,e})$. The iterative process then consists in computing the step of temperature ΔT^i and pressure ΔP^i so that the updated values (T^{i+1}, P^{i+1}) and corresponding values of $(\rho_\ell^{i+1}, \rho_v^{i+1}, e_{s,\ell}^{i+1}, e_{s,v}^{i+1})$ minimize both the difference $\left(F_\ell^{i+1} - F_v^{i+1}\right)$ between liquid and vapour phases and the difference $(\alpha_{\ell,\rho}^{i+1} - \alpha_{\ell,e}^{i+1})$. In this respect, steps are built as:

$$\begin{cases} F_\ell^i + \Delta F_\ell^i = F_v^i + \Delta F_v^i & \text{(11a)} \\ \alpha_{\ell,\rho}^i + \Delta \alpha_{\ell,\rho}^i = \alpha_{\ell,e}^i + \Delta \alpha_{\ell,e}^i. & \text{(11b)} \end{cases}$$

The detail of thermodynamic quantities such as the fugacity for cubic EoS is recalled in appendix A). The variations of both $\alpha_{\ell,\rho}$ and $\alpha_{\ell,e}$ can be expressed from $(\Delta P, \Delta T)$ using a first-order approximation:

$$\Delta \alpha_\ell \approx \left.\frac{\partial \alpha_\ell}{\partial P}\right|_T \Delta P + \left.\frac{\partial \alpha_\ell}{\partial T}\right|_P \Delta T \tag{12}$$

The pressure step is then computed as

$$\Delta P^i = \underbrace{\frac{\left.\frac{\partial \alpha_{\ell,\rho}}{\partial T}\right|_P - \left.\frac{\partial \alpha_{\ell,e}}{\partial T}\right|_P}{\left.\frac{\partial \alpha_{\ell,\rho}}{\partial P}\right|_T - \left.\frac{\partial \alpha_{\ell,e}}{\partial P}\right|_T}}_{\eta_T} \Delta T^i - \underbrace{\frac{\alpha_{\ell,\rho}^i - \alpha_{\ell,e}^i}{\left.\frac{\partial \alpha_{\ell,\rho}}{\partial P}\right|_T - \left.\frac{\partial \alpha_{\ell,e}}{\partial P}\right|_T}}_{\eta_\alpha}, \tag{13}$$

with ΔT^i given by

$$\Delta T^i = \frac{\left(F_v^i - F_\ell^i\right) + \left(\left.\frac{\partial F_\ell}{\partial P}\right|_T - \left.\frac{\partial F_v}{\partial P}\right|_T\right)\eta_\alpha}{\left(\left.\frac{\partial F_\ell}{\partial T}\right|_P - \left.\frac{\partial F_v}{\partial T}\right|_P\right) - \left(\left.\frac{\partial F_\ell}{\partial P}\right|_T - \left.\frac{\partial F_v}{\partial P}\right|_T\right)\eta_T}. \tag{14}$$

Partial derivatives that appear in the previous expressions are detailed in appendix A.

These steps of pressure and temperature are made until a certain level of convergence is reached towards the cancellation of the two errors $\left|\alpha_{\ell,\rho} - \alpha_{\ell,e}\right|$ and $|F_\ell - F_v|$.

The initialization is designed to give the best possible estimate for (T, P). To do this, one tries to compute a two-phase equilibrium verified by the values of transported density and previous time step temperature (ρ, T_{old}). If this couple corresponds to a two-phase state, T_{old} together with the computed pressure are taken as the first-guess. Otherwise, a two phase equilibrium is computed from the couple (ρ, T_m) and is used as the first guess.

Along the iterations, it is necessary to make a few verifications to ensure that the loop evolves properly. First, if the pressure step computed from (13) yields a negative pressure, it is reduced until it provides a positive pressure. This is likely to happen near pure liquid states, especially at low temperatures, where the pressure sensitivity to density variations is strong. It is also important to ensure that pressure and temperature steps do not yield a one-phase state. Otherwise, the steps are reduced until a two-phase point is reached.

3 Mathematical Properties

This section aims at providing the derivation of the important mathematical properties of the Homogeneous Equilibrium Model. This is particularly interesting towards the implementation into the solver AVBP (see for example [11], for more details). AVBP is a multispecies compressible unsteady solver jointly developed by CERFACS and IFPEN.

3.1 Jacobian Matrices

Among the numerical methods available in this solver, Two-Step Taylor-Galerkin methods (TTGC, TTG4A [4]) are particularly interesting as they provide a third-order convergence in space and time for a limited computational cost. Their derivation uses the so-called Cauchy-Kowalevski process, which requires to compute the Jacobian matrix of the flux function (2), given by:

$$J_{\mathscr{F}}(U) = \left(\left.\frac{\partial \mathscr{F}(U)_i}{\partial U_j}\right|_{U_{k,\ k\neq j}} \right)_{i,j}. \tag{15}$$

After some developments, this matrix reduces to the following form:

$$J_{\mathscr{F}}(U) = \begin{pmatrix} 0 & 1 & 0 \\ \left(\frac{b}{2}-1\right)u^2 - ab & (2-b)\,u & b \\ \left(b\frac{u^2}{2} - abu - h_s\right)u & h_s - bu^2 & (1+b)\,u \end{pmatrix} \tag{16}$$

with coefficients a and b defined by:

$$\begin{cases} a = \left.\dfrac{\partial \rho e_s}{\partial \rho}\right|_P & \text{(17a)} \\ b = \left.\dfrac{\partial P}{\partial \rho e_s}\right|_\rho & \text{(17b)} \end{cases}$$

Expression (16) is valid for any thermodynamic closure. In the supercritical or one-phase domain, the usual form of the Jacobian matrix for cubic EoS naturally applies [18]. For points lying in the binodal region, as phase separation is considered by the equilibrium model, the derivation of partial derivatives at saturation is necessary.

First, the calculation of $\left.\frac{\partial(\rho e_s)}{\partial \rho}\right|_P$ is presented. To achieve this, it is worth mentioning that the single-phase quantities $\rho_\ell, \rho_v, e_{s,\ell}, e_{s,v}$ are function of the pressure only. Hence the derivative of liquid volume fraction with respect to mixture density, from (9a), which writes:

$$\left.\frac{\partial \alpha_\ell}{\partial \rho}\right|_P = \frac{1}{\rho_\ell - \rho_v}. \tag{18}$$

Then the calculation can be achieved by differentiating (8b), which eventually yields:

$$a = \frac{\rho_\ell e_{s,\ell} - \rho_v e_{s,v}}{\rho_\ell - \rho_v}. \tag{19}$$

To treat the derivation of the other term $\left.\frac{\partial(\rho e_s)}{\partial \rho}\right|_P$, it is necessary to introduce *saturation derivatives*, which, for a thermodynamic quantity ψ usually expressed as a function of pressure and temperature, write:

$$\left.\frac{\partial \psi}{\partial P}\right|_{\text{sat}} = \left.\frac{\partial \psi}{\partial P}\right|_T + \left.\frac{\partial \psi}{\partial T}\right|_P \left.\frac{\partial T}{\partial P}\right|_{\text{sat}}. \tag{20}$$

The derivative of temperature with respect to pressure at saturation is given by the well-known Clausius-Clapeyron relation [19] and is denoted here ϑ:

$$\vartheta = \left.\frac{\partial T}{\partial P}\right|_{\text{sat}} = \frac{T(\rho_\ell - \rho_v)}{\rho_v \rho_\ell (h_{s,v} - h_{s,\ell})}. \tag{21}$$

One can then differentiate (8b) with respect to pressure, which writes:

$$\left.\frac{\partial \rho e_s}{\partial P}\right|_\rho = (\rho_\ell e_{s,\ell} - \rho_v e_{s,v}) \left.\frac{\partial \alpha_\ell}{\partial P}\right|_{\rho,\text{sat}} + \sum_{k\in\{\ell,v\}} \left[\alpha_k \rho_k \left.\frac{\partial e_{s,k}}{\partial P}\right|_{\text{sat}} + \alpha_k e_{s,k} \left.\frac{\partial \rho_k}{\partial P}\right|_{\text{sat}}\right] \tag{22}$$

In this expression, saturation derivatives for single-phase thermodynamic quantities appear and can be computed using (20) and the cubic EoS for each phase. This writes eventually:

$$b = \left(\left.\frac{\partial \rho e_s}{\partial P}\right|_\rho\right)^{-1} = \frac{1}{\vartheta C_{p,\text{mix}} + \left(\frac{\beta_{\text{mix}}}{\vartheta} - 2\alpha^T_{\text{mix}}\right)T} \tag{23}$$

where $C_{p,\text{mix}} = \alpha_\ell \rho_\ell c_{p,\ell} + (1-\alpha_\ell)\rho_v c_{p,v}$ is the mixture volume-specific isobaric heat capacity, $\alpha^T_{\text{mix}} = \alpha_\ell \alpha^T_\ell + (1-\alpha_\ell)\alpha^T_v$ is a mixture thermal expansion coefficient and $\beta_{\text{mix}} = \alpha_\ell \beta_\ell + (1-\alpha_\ell)\beta_v$ a mixture isothermal compressibility coefficient. In the previous expressions, for each phase $k \in \{\ell, v\}$ appear the thermal expansion and isothermal compressibility coefficients (defined in appendix A.1) and the specific isobaric heat capacity $c_{p,k} = \left.\frac{\partial h_{s,k}}{\partial T}\right|_P$, with sensible enthalpy $h_{s,k} = e_{s,k} + \frac{P}{\rho_k}$.

3.2 Speed of Sound and Characteristic Boundary Conditions

Once the Jacobian matrix has been calculated, its diagonalization yields important mathematical properties of the model. This allows to compute the speed of sound and verify the hyperbolicity of the PDE and also to derive the so-called Characteristic Boundary Conditions introduced by Poinsot and Lele [18].

In the first place, it is helpful to write system (1) in its non-conservative pseudo-linearized form, in terms of primitive variables $V = (\rho, u, P)^T$. This reads:

$$\frac{\partial V}{\partial t} + J^p_{\mathscr{F}}(V)\frac{\partial V}{\partial x} = 0, \tag{24}$$

with the Jacobian matrix expressed this time in primitive variables (after change of basis):

$$J^p_{\mathscr{F}}(V) = \begin{pmatrix} u & \rho & 0 \\ 0 & u & \frac{1}{\rho} \\ 0 & \rho b(h_s - a) & u \end{pmatrix}. \tag{25}$$

This form once again stands for any thermodynamic closure. h_s here indicates the specific sensible enthalpy $h_s = e_s + P/\rho$. The term $b(h_s - a)$ can be expressed under the form:

$$b(h_s - a) = \left.\frac{\partial P}{\partial \rho}\right|_s + \left.\frac{\partial P}{\partial e_s}\right|_\rho \left(\frac{P}{\rho^2} - \left.\frac{\partial e_s}{\partial \rho}\right|_s\right), \tag{26}$$

where s is the specific entropy of the two-phase mixture. In order for this term to reduce to $\left.\frac{\partial P}{\partial \rho}\right|_s$, Gibbs relation must be verified by the thermodynamic closure. This is obviously true for cubic EoS and is also verified by the homogeneous equilibrium closure, as shown in the following. Euler theorem and Gibbs-Duhem relations for each phase $k \in \{\ell, v\}$ write:

$$\begin{cases} \mathscr{E}_{s,k} = T\mathscr{S}_k - P\mathscr{V}_k + gm_k & \text{(27a)} \\ \mathscr{S}_k \,\mathrm{d}T - \mathscr{V}_k \,\mathrm{d}P + m_k \,\mathrm{d}g = 0 & \text{(27b)} \end{cases}$$

where $\mathscr{E}_{s,k}$, $\mathscr{S}_k$, $\mathscr{V}_k$ and m_k are respectively the extensive sensible energy, entropy, volume and mass of phase k. Summing over both phases, one gets

$$\begin{cases} \mathscr{E}_s = T\mathscr{S} - P\mathscr{V} + gm & \text{(28a)} \\ \mathscr{S} \,\mathrm{d}T - \mathscr{V} \,\mathrm{d}P + m \,\mathrm{d}g = 0 & \text{(28b)} \end{cases}$$

with $\mathscr{E}_s$, $\mathscr{S}$, $\mathscr{V}$ and m respectively the extensive sensible energy, entropy, volume and mass of the thermodynamic system that constitute the ensemble of both phases. One observes that Gibbs-Duhem relation (28b) is immediately verified by the two-phase mixture at equilibrium. Dividing (28a) and (28b) by the mixture mass m and differentiating the first relation yield Gibbs relation for the two-phase mixture at homogeneous equilibrium :

$$\mathrm{d}e_s = T\,\mathrm{d}s + \frac{P}{\rho^2}\,\mathrm{d}\rho \tag{29}$$

Thus, the well-known form of the Jacobian matrix in primitive variables is still valid for the two-phase mixture:

$$J^p_{\mathscr{F}}(V) = \begin{pmatrix} u & \rho & 0 \\ 0 & u & \frac{1}{\rho} \\ 0 & \rho c^2 & u \end{pmatrix}, \tag{30}$$

where the speed of sound appears to have the same definition

$$c = \sqrt{\left.\frac{\partial P}{\partial \rho}\right|_s}, \tag{31}$$

except that ρ and s are, in the binodal region, variables of the two-phase mixture at equilibrium. The mixing law for specific entropy is:

$$\rho s = \alpha_\ell \rho_\ell s_\ell + (1 - \alpha_\ell)\rho_v s_v. \tag{32}$$

The calculation of the speed of sound in the two-phase case can be achieved by expressing the differential of specific entropy from density and pressure differentials. These developments provide the following form for the speed of sound to the square:

$$c^2 = \frac{1}{\rho\left(\frac{\vartheta^2}{T}C_{p,\mathrm{mix}} - 2\alpha^T_{\mathrm{mix}}\vartheta + \beta_{\mathrm{mix}}\right)}. \tag{33}$$

Although this compact form does not directly show the positivity of c^2, it is actually verified, as shown in [6]. As expected, this thermodynamic closure effectively allows the flow model to be hyperbolic in both subcritical and supercritical regions.

Diagonalization of the Jacobian $J^p_{\mathscr{F}}(V)$ yields the so-called characteristic form. The characteristic Jacobian Matrix $J^c_{\mathscr{F}}(W)$ can be expressed using transformation matrices $L_U = R_U^{-1}$ as:

$$J^c_{\mathscr{F}}(W) = L_U J_{\mathscr{F}}(U) R_U, \tag{34}$$

these transformation matrices allowing to change basis between conservative and characteristic variables:

$$\begin{cases} \partial W = L_U \partial U, & \text{(35a)} \\ \partial U = R_U \partial W. & \text{(35b)} \end{cases}$$

As a consequence of $J^p_{\mathscr{F}}(V)$ taking the usual form despite the two phase closure, its diagonalized form remains similar to its one-phase counterpart, as diagonalization yields:

$$J^c_{\mathscr{F}}(W) = \begin{pmatrix} u & 0 & 0 \\ 0 & u+c & 0 \\ 0 & 0 & u-c \end{pmatrix} \tag{36}$$

with

$$L_U = \frac{b}{\rho c} \begin{pmatrix} \rho c(-u^2/2+1+a) & \rho c u & \rho c \\ u^2/2 + \frac{uc}{b} - a & -\left(u+\frac{c}{b}\right) & 1 \\ u^2/2 - \frac{uc}{b} - a & -\left(u-\frac{c}{b}\right) & 1 \end{pmatrix}, \tag{37a}$$

$$R_U = \frac{\rho}{2c} \begin{pmatrix} \frac{2c}{\rho} & 1 & 1 \\ \frac{2cu}{\rho} & u+c & u-c \\ \frac{2c}{\rho}\left(\frac{u^2}{2}+a\right) & \frac{u^2}{2}+a+c\left(\frac{c}{b}+u\right) & \frac{u^2}{2}+a+c\left(\frac{c}{b}-u\right) \end{pmatrix}. \tag{37b}$$

One observes that the modifications needed to write the Characteristic Boundary Conditions in the two-phase case reduce to modifying thermodynamic coefficients a, b and c (the speed of sound), according to (19), (23) and (33). From this point, test cases are run to observe the behaviour of the homogeneous equilibrium model.

4 Test Cases, Results and Discussion

This section is dedicated to the different test cases that have been studied. All computations were performed on the solver AVBP-RG (see [21–23,25,26] among others), the real-gas version of AVBP. The numerical method used here is TTG4A, a two-step Taylor-Galerkin method [4]. The fluid considered in the following is pure nitrogen with tabulated isochoric heat capacity.

4.1 One-dimensional test cases

In order to validate the formulations of the Jacobian matrix and the corresponding characteristic boundary conditions, it is interesting to study the behaviour of acoustic and entropy perturbations in a 1D domain, bounded by fully reflecting boundary conditions or fully non-reflecting boundary conditions.

Case 1 - Acoustic Waves with Fully Reflecting Boundary Conditions: a uniform 100-node mesh is used, on a domain $\Omega = [0, L]$ of length $L = 10^{-2}$ m. The initial condition used in this case is built by adding gaussian perturbations on the characteristic variables associated to the forward and backward acoustic eigenvalues $\partial W^+(x) = \partial W^-(x) = \exp\left(-200\left(x - L/2\right)^2\right)$ to the homogeneous two-phase solution U_0. U_0 is the set of conservative variables corresponding to density $\rho_0 = 100\ kg/m^3$, pressure $P_0 = 10\ bar$ and velocity $u_0 = 0\ m/s$. Initial solution is then

$$U(x, t=0) = U_0 + R_{U_0} \cdot \begin{pmatrix} 0 \\ \partial W^+(x) \\ \partial W^-(x) \end{pmatrix}. \tag{38}$$

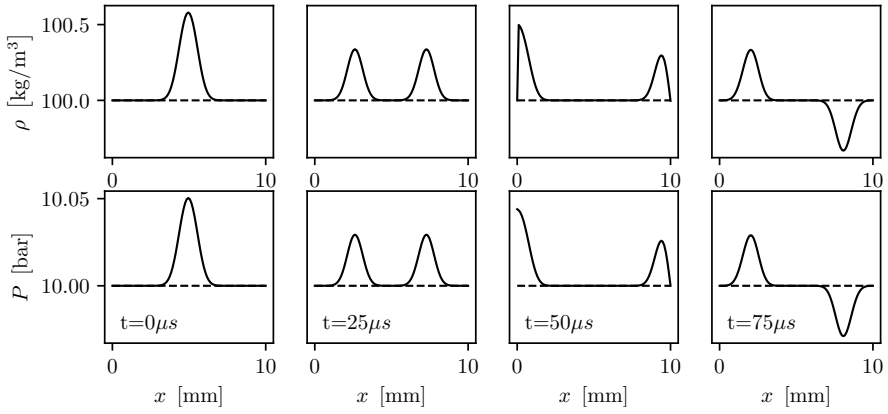

Fig. 2: Test case 1 – Initially superimposed backward and forward acoustic waves with fully reflecting boundary conditions. Density and pressure snapshots of the solution. From left to right: initial time, before, during and after interaction with domain boundaries.

The boundary conditions considered here are a fully reflecting inlet with u and ρ imposed on the left-hand side and a fully reflecting outlet with pressure imposed on the right hand side. Their formulation is described in appendix B.

The results are displayed in Fig. 2. Acoustic waves follow the expected behaviour, as their amplitude is preserved. As observed, imposing pressure on the outlet results in reflecting into the domain an acoustic wave of opposite sign. On the contrary, imposing velocity at the inlet results in reflecting into the domain an acoustic wave of same sign.

Case 2 - Entropy Wave with Fully Reflecting Boundary Conditions: This case is built on the same setup as the previous one. The initial condition is now an entropy perturbation $\partial W^s(x) = 10\exp\left(-200\left(x-L/2\right)^2\right)$ added to the homogeneous solution U_0. U_0 is now the set of conservative variables corresponding to density $\rho_0 = 50\ kg/m^3$, pressure $P_0 = 10\ bar$ and velocity $u_0 = 40\ m/s$. Initial solution is then computed as:

$$U(x,t=0) = U_0 + R_{U_0} \cdot \begin{pmatrix} \partial W^s(x) \\ 0 \\ 0 \end{pmatrix}. \tag{39}$$

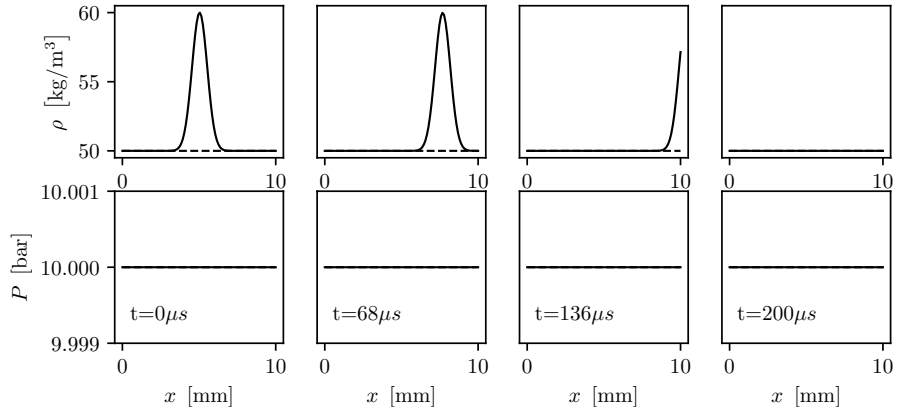

Fig. 3: Test case 2 – Entropy wave transport with fully reflecting characteristic boundary conditions. Density and pressure snapshots of the solution. From left to right: initial time, before, during and after interaction with domain boundaries.

Results are displayed on Fig. 3. The entropy wave is well convected and evacuated by the outlet boundary condition, without generating any acoustic noise.

Case 3 - Acoustic Wave with Non-Reflecting Outlet and Fully Reflecting Inlet: For this test case, the initial solution (38) is used, as for *Case 1*. Here, boundary conditions are the relaxed outlet for pressure on the right-hand side and a fully-reflecting inlet with imposed density and velocity on the left-hand side.

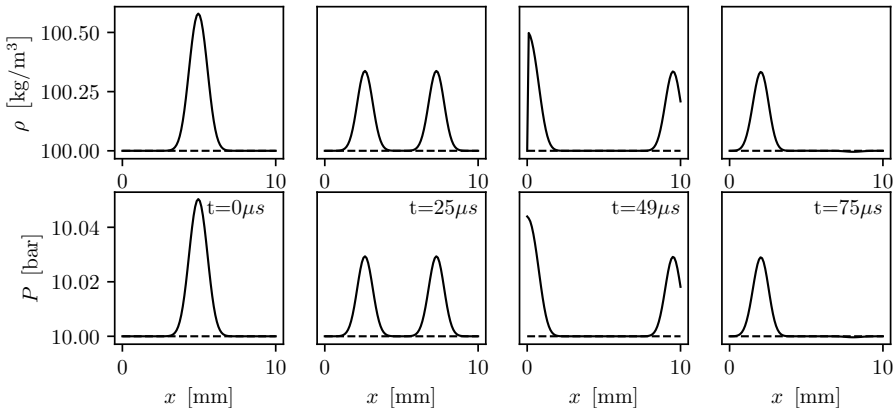

Fig. 4: Test case 3 – Acoustic wave transport with non-reflecting characteristic boundary condition on the right-hand side. Density and pressure snapshots of the solution. From left to right: initial time, before, during and after interaction with domain boundaries.

The results for this test case are shown in Fig. 4. Once again, the expected behaviour is observed, as the wave hitting the outlet is evacuated, the backward acoustic wave being reflected on the inlet.

The present section allowed to validate the derivation and implementation of the boundary conditions in one dimension. The following section is then dedicated to multidimensional computations.

4.2 Two-dimensional test cases

In this section, the behaviour of the thermodynamic closure is investigated in a multidimensional framework. Extending previous developments to multidimensional systems presents no difficulty, as the modifications of the Jacobian matrices remain constrained to the thermodynamic coefficients. The form of the useful matrices can be found in Appendix B.

Case 4 - Fully two-phase "droplet" evacuation: For this test case, pressure and velocity are initially homogeneous in a square domain $\Omega = [-L/2, L/2] \times [-L/2, L/2]$, with respective values $P_0 = 10\ bar$, $u_0 = 40\ m/s$ and $v_0 = 0\ m/s$. Length of the domain is $L = 10^{-2} m$, discretized over 100×100 points. Density profile is built as

$$\rho_0(x,y) = \frac{\rho_{\max} + \rho_{\min}}{2} + \left(\frac{\rho_{\min} - \rho_{\max}}{2}\right) \tanh\left(70\left(\sqrt{x^2+y^2} + 0.3\right)\right), \tag{40}$$

with $\rho_{\min} = 50 kg/m^3$ and $\rho_{\max} = 600 kg/m^3$. These parameters correspond to a liquid-phase mass fraction ranging from $Y_{\ell,\min} = 0.188$ to $Y_{\ell,\max} = 0.996$.

Results are displayed in Fig. 5. The density perturbation exits the domain, as no acoustic noise is generated.

Case 5 - Enforcing Velocity Profile: This test case aims at validating the behaviour of characteristic boundary conditions with relaxation towards a given value. In the same domain as case 4, the solution is initialized with values $\rho_0 = 300\ kg/m^3$, $P_0 = 10\ bar$, $u_0 = 30\ m/s, v_0 = 0\ m/s$. At time $t = 0s$, horizontal velocity and density profiles are enforced on the inlet. To do this, on the left side of the domain, an inlet with relaxation towards imposed density and velocity is used together with an outlet, on the right boundary, with relaxation towards imposed pressure (see appendix B). Top and bottom boundary conditions are no-slip walls. Relaxation coefficients at the boundaries, on ρ, u and P are set to 40. Velocity and density profiles are defined by the following formula, the resulting values being centered on the homogeneous field values ρ_0 and u_0:

$$\begin{cases} u_{\text{inlet}} = u_0 \left(1 + \dfrac{1}{2}\tanh(10^3 y)\right) & \text{(41a)} \\ \rho_{\text{inlet}} = \rho_0 \left(1 - \dfrac{1}{2}\tanh(10^3 y)\right) & \text{(41b)} \end{cases}$$

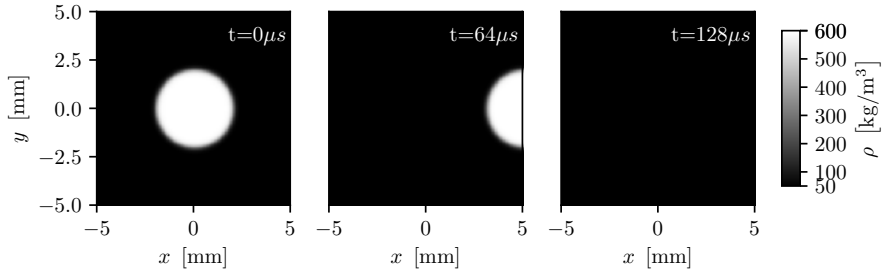

(a) Density snapshots, taken before, during and after the droplet hits the outlet.

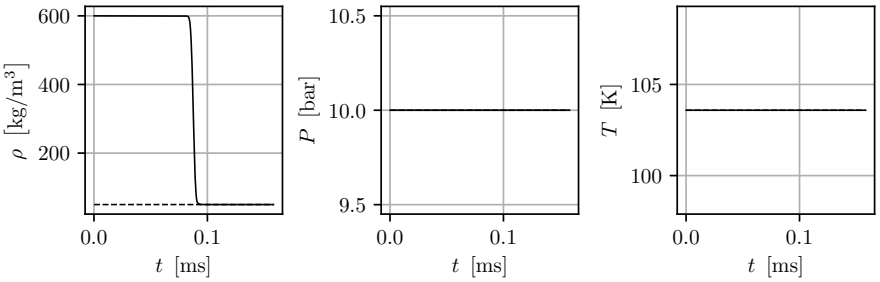

(b) Temporal evolution of minimum (dashed lines) and maximum (solid lines) values of density, pressure and temperature. Pressure and temperature remain constant and homogeneous in the domain, as the density perturbation is evacuated.

Fig. 5: Test case 4 – Transport of a droplet-like solution.

Results are displayed in Figure 6. After a transient regime, each flow quantity stabilizes towards its expected value. The final profile of velocity corresponds to the prescribed form.

5 Conclusion and Prospects

The present article presents the Homogeneous Equilibrium Method as a thermodynamic closure to extend the use of Cubic EoS to a subcritical region, in the case of a monospecies fluid. The practical implementation of the equilibrium computation has been described and the mathematical properties have been investigated, to provide the flow model's Jacobian matrix together with its corresponding Characteristic Boundary Conditions implementation. In particular, it has been observed that the form of the resulting flow model is similar to the usual one-phase case, which makes its implementation more simple. Test cases were presented to validate both the derivation and implementation of the thermodynamic closure. These test cases illustrate that the obtained flow model is suited for computations using classical hyperbolic PDEs numerical methods, in particular of the Taylor-Galerkin family.

Current and future developments focus on the extension of the thermodynamic closure and its mathematical properties to multispecies mixtures, assuming one-fluid mixture using the Corresponding States Principle [19]. Then, implementation of a surface tension model is the next step towards the development of a solver able to handle the whole range of pressure encountered in industrial combustors such as rocket and Diesel engines.

Acknowledgements The authors acknowledge funding from ANR through project ANR-14-CE22-0014 (SUBSUPERJET)

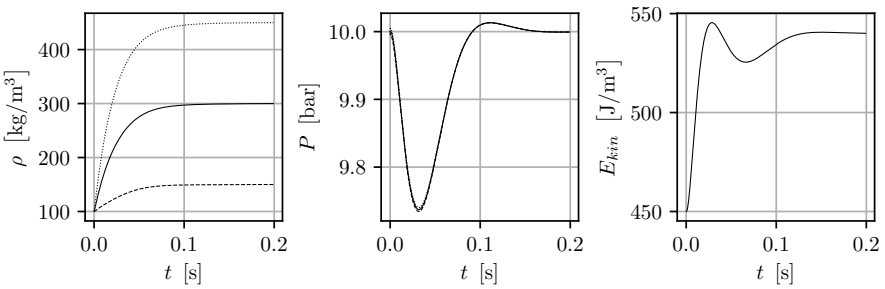

(a) Left-hand side figure shows the evolution of minimum (dashed line), maximum (dotted line) and mean density (solid line) in the domain. Center figure represents the evolution of minimum (dashed line), maximum (dotted line) and mean pressure (solid line) in the domain. Right-hand side figure shows the evolution of mean kinetic energy in the domain.

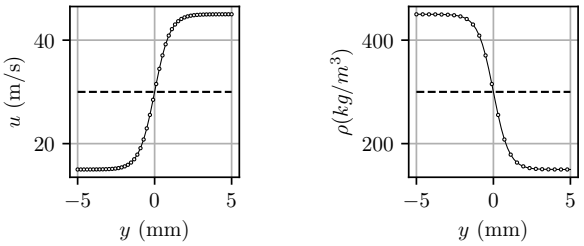

(b) velocity and density profiles at the inlet: initial (dashed lines), target (solid lines) and final values (symbols).

Fig. 6: Test case 5 – Relaxation towards prescribed density and velocity profiles at the inlet. Final time is 0.2 s.

Appendix

A Thermodynamic developments

A.1 Thermodynamic Definitions

Useful thermodynamic definitions for cubic EoS are recalled in this appendix.

Thermal expansion coefficient α^T is defined by:

$$\alpha^T = -\frac{1}{\rho}\left.\frac{\partial \rho}{\partial T}\right|_P \tag{42}$$

Isothermal compressibility coefficient β is defined by:

$$\beta = \frac{1}{\rho}\left.\frac{\partial \rho}{\partial P}\right|_T \tag{43}$$

Entropy is defined by adding a residual value to s^{PG}, the entropy predicted by the Perfect-Gas EoS, through the relation:

$$s(T,P) = s^{\mathrm{PG}}(T,P) + \int_{P_0}^{P}\left[\frac{1}{\rho^2}\left.\frac{\partial \rho}{\partial T}\right|_{P_*} - \frac{r}{P_*}\right]\mathrm{d}P_*. \tag{44}$$

Fugacity f is defined by the relation:

$$rT\ln\left(\frac{f(\rho,T)}{P}\right) = \int_{\rho_0}^{\rho}\left[\frac{P}{\rho_*^2} - \frac{rT}{\rho_*}\right]\mathrm{d}\rho_* - rT\ln\left(\frac{P}{\rho rT}\right) + \frac{P}{\rho} - rT = g_{\mathrm{res}}(\rho,T), \tag{45}$$

where $g_{\mathrm{res}}(\rho,T)$ is the residual Gibbs free energy, representing the difference between the value of $g(\rho,T)$ predicted by the considered cubic EoS and the one predicted by the Perfect-Gas EoS.

A.2 Useful Partial Derivatives

In order to derive the pressure (13) and temperature (14) steps used in the iterative loop, partial derivatives of the quantity F are needed. They write:

$$\begin{cases} \left.\dfrac{\partial F}{\partial T}\right|_P = \dfrac{1}{T}\left[\ln(\rho rT) - F + \displaystyle\int_0^{\rho}\left(\frac{1}{r\rho_*^2}\frac{\alpha^T}{\beta} - \frac{1}{\rho_*}\right)\mathrm{d}\rho_*\right] & \text{(46a)} \\ \left.\dfrac{\partial F}{\partial P}\right|_T = \dfrac{1}{\rho rT} & \text{(46b)} \end{cases}$$

For the computation of mixture fraction $\alpha_{\ell,e}$ derivatives with respect to temperature and pressure, the following relations are needed:

$$\begin{cases} \left.\dfrac{\partial e_s}{\partial P}\right|_T = \dfrac{1}{\rho}\left(\beta P - \alpha^T T\right) & \text{(47a)} \\ \left.\dfrac{\partial e_s}{\partial T}\right|_P = c_v + \dfrac{\alpha^T}{\rho\beta}\left(\alpha^T T - \beta P\right) & \text{(47b)} \end{cases}$$

B Characteristic boundary conditions

In this appendix are recalled the derivation and implementation of characteristic boundary conditions.

B.1 Transformation Matrices

Transformation matrices between the different sets of flow variables are recalled here. First, transformation matrices to change basis from a primitive variation ∂V to characteristic perturbation ∂W are given by:

$$L_V = \begin{pmatrix} 1 & 0 & 0 & 0 & -\frac{1}{c^2} \\ 0 & n_x & n_y & n_z & \frac{1}{\rho c} \\ 0 & -n_x & -n_y & -n_z & \frac{1}{\rho c} \\ 0 & t_{1x} & t_{1y} & t_{1z} & 0 \\ 0 & t_{2x} & t_{2y} & t_{2z} & 0 \end{pmatrix} \tag{48}$$

$$R_V = \begin{pmatrix} 1 & \frac{\rho}{2c} & \frac{\rho}{2c} & 0 & 0 \\ 0 & \frac{n_x}{2} & -\frac{n_x}{2} & t_{1x} & t_{2x} \\ 0 & \frac{n_y}{2} & -\frac{n_y}{2} & t_{1y} & t_{2y} \\ 0 & \frac{n_z}{2} & -\frac{n_z}{2} & t_{1z} & t_{2z} \\ \frac{\rho c}{2} & \frac{\rho c}{2} & 0 & 0 & 0 \end{pmatrix} \tag{49}$$

These matrices include the rotation of the frame in order to express velocities in a frame that includes the normal to the boundary $\mathbf{n} = \left[n_x, n_y, n_z\right]^t$. $\mathbf{t_1} = \left[t_{1x}, t_{1y}, t_{1z}\right]^t$ and $\mathbf{t_2} = \left[t_{2x}, t_{2y}, t_{2z}\right]^t$ denote the two vectors of the basis that are tangential to the boundary. The velocity writes $\mathbf{u} = [u, v, w]^t$

Eventually, the transformation matrices to change basis from conservative to characteristic including rotation of the frame for boundary condition applications, in three dimensions, write:

$$L_U = \begin{pmatrix} 1 + \frac{b(a-e_c)}{c^2} & \frac{bu}{c^2} & \frac{bv}{c^2} & \frac{bw}{c^2} & -\frac{b}{c^2} \\ -\frac{\mathbf{u}\cdot\mathbf{t_1}}{\rho} & \frac{t_{1x}}{\rho} & \frac{t_{1y}}{\rho} & \frac{t_{1z}}{\rho} & 0 \\ -\frac{\mathbf{u}\cdot\mathbf{t_2}}{\rho} & \frac{t_{2x}}{\rho} & \frac{t_{2y}}{\rho} & \frac{t_{2z}}{\rho} & 0 \\ \frac{1}{\rho}\left(\frac{b(e_c-a)}{c} - \mathbf{u}\cdot\mathbf{n}\right) & -\frac{bu-cn_x}{\rho c} & -\frac{bv-cn_y}{\rho c} & -\frac{bw-cn_x}{\rho c} & \frac{b}{\rho c} \\ \frac{1}{\rho}\left(\frac{b(e_c-a)}{c} + \mathbf{u}\cdot\mathbf{n}\right) & -\frac{bu+cn_x}{\rho c} & -\frac{bv+cn_y}{\rho c} & -\frac{bw+cn_x}{\rho c} & \frac{b}{\rho c} \end{pmatrix} \tag{50}$$

$$R_U = \begin{pmatrix} 1 & 0 & 0 & \frac{\rho}{2c} & \frac{\rho}{2c} \\ u & \rho t_{1x} & \rho t_{2x} & \frac{\rho}{2c}(u + cn_x) & \frac{\rho}{2c}(u - cn_x) \\ v & \rho t_{1y} & \rho t_{2y} & \frac{\rho}{2c}(v + cn_y) & \frac{\rho}{2c}(v - cn_y) \\ w & \rho t_{1z} & \rho t_{2z} & \frac{\rho}{2c}(w + cn_z) & \frac{\rho}{2c}(w - cn_z) \\ e_c + a & \rho\mathbf{u}\cdot\mathbf{t_1} & \rho\mathbf{u}\cdot\mathbf{t_2} & \frac{\rho}{2c}\left(e_c + a + c\mathbf{u}\cdot\mathbf{n} + \frac{c^2}{b}\right) & \frac{\rho}{2c}\left(e_c + a - c\mathbf{u}\cdot\mathbf{n} + \frac{c^2}{b}\right) \end{pmatrix} \tag{51}$$

B.2 Inlets with prescribed density and velocity

In the following, fully reflecting characteristic boundary conditions are briefly described in the case of subsonic flows, in one dimension. More details about characteristic boundary conditions can be found in [18]. In order to impose velocity and density on an inlet, one would modify the flow quantities predicted by the numerical transport (denoted here with superscript ^{p}) to ensure that the corrected values (denoted with superscript ^{c}) of ρ^c and u^c are equal to the target values ρ^t and u^t. If the previous values at the boundaries are ρ^0 and u^0, the variations $\partial\rho = \rho^c - \rho^0$ and $\partial u = u^c - u^0$ must be cancelled. In terms of characteristic variables, applying the transformations mentioned in previous section B.1, one gets:

$$\begin{cases} \left(\partial W^s\right)^p = (\partial\rho)^p + \dfrac{1}{c^2}(\partial P)^p & \text{(52a)} \\ \left(\partial W^+\right)^p = (\partial u)^p + \dfrac{1}{\rho c}(\partial P)^p & \text{(52b)} \\ \left(\partial W^-\right)^p = -(\partial u)^p + \dfrac{1}{\rho c}(\partial P)^p & \text{(52c)} \end{cases}$$

At a subsonic inlet, only the inward acoustic wave ∂W^- information is known from inside of the domain. Thus, the entropy wave ∂W^s and outward acoustic wave ∂W^+ must be corrected in order to ensure that density and velocity remain constant. Hence the corrected values:

$$\begin{cases} \left(\partial W^+\right)^c = \left(\partial W^-\right)^p & \text{(53a)} \\ \left(\partial W^s\right)^c = -\dfrac{\rho}{c}\left(\partial W^-\right)^p & \text{(53b)} \end{cases}$$

Actually, to prevent density and velocity drift at the boundary, the correction is defined as

$$\begin{cases} \left(\partial W^+\right)^c = \left(\partial W^-\right)^p + 2(u^t - u^p) & \text{(54a)} \\ \left(\partial W^s\right)^c = -\dfrac{\rho}{c}\left(\partial W^- + (u^t - u)\right)^p + (\rho^t - \rho^p) & \text{(54b)} \end{cases}$$

B.3 Outlet with prescribed pressure

To build up a subsonic fully reflecting pressure outlet, one would modify the predicted flow quantities to ensure that the corrected value P^c is equal to the target value P^t. If the previous values at the boundaries are P^0, the variation $\partial P = P^c - P^0$ has to be cancelled.

At a subsonic outlet, only the outward acoustic wave ∂W^+ information may be corrected, as the two other waves carry information from inside the domain. From equations 52, correction writes:

$$\left(\partial W^-\right)^c = -\left(\partial W^+\right)^p \tag{55}$$

Actually, to ensure that no boundary pressure drift is observed, correction is defined as

$$\left(\partial W^+\right)^c = \left(\partial W^-\right)^p + 2\frac{(P^t - P^p)}{\rho c}. \tag{56}$$

References

1. Baer, M., Nunziato, J.: A two-phase mixture theory for the deflagration-to-detonation transition (ddt) in reactive granular materials. International Journal of Multiphase Flow **12**(6), 861 – 889 (1986). DOI http://dx.doi.org/10.1016/0301-9322(86)90033-9. URL http://www.sciencedirect.com/science/article/pii/0301932286900339
2. Candel, S., Juniper, M., Singla, G., Scouflaire, P., Rolon, C.: Structure and dynamics of cryogenic flames at supercritical pressure. Combustion Science and Technology **178**(1-3), 161–192 (2006). DOI 10.1080/00102200500292530. URL http://dx.doi.org/10.1080/00102200500292530
3. Chiapolino, A., Boivin, P., Saurel, R.: A simple phase transition relaxation solver for liquid-vapor flows. International Journal for Numerical Methods in Fluids pp. 1–42 (2016). DOI 10.1002/fld.4282
4. Colin, O., Rudgyard, M.: Development of High-Order Taylor–Galerkin Schemes for LES. Journal of Computational Physics **162**(2), 338–371 (2000). DOI 10.1006/jcph.2000.6538. URL http://www.sciencedirect.com/science/article/pii/S0021999100965380
5. Desjardins, O., Moureau, V., Pitsch, H.: An accurate conservative level set/ghost fluid method for simulating turbulent atomization. Journal of Computational Physics **227**(18), 8395 – 8416 (2008). DOI https://doi.org/10.1016/j.jcp.2008.05.027. URL http://www.sciencedirect.com/science/article/pii/S0021999108003112
6. Flåtten, T., Lund, H.: Relaxation Two-Phase Flow Models and the Subcharacteristic Condition. Mathematical Models and Methods in Applied Sciences **21**(12), 2379–2407 (2011). DOI 10.1142/S0218202511005775. URL http://www.worldscientific.com/doi/abs/10.1142/S0218202511005775
7. Hakim, L., Ruiz, A., Schmitt, T., Boileau, M., Staffelbach, G., Ducruix, S., Cuenot, B., Candel, S.: Large eddy simulations of multiple transcritical coaxial flames submitted to a high-frequency transverse acoustic modulation. Proceedings of the Combustion Institute **35**(2), 1461 – 1468 (2015). DOI https://doi.org/10.1016/j.proci.2014.05.142. URL http://www.sciencedirect.com/science/article/pii/S154074891400145X
8. Kapila, A.K., Menikoff, R., Bdzil, J.B., Son, S.F., Stewart, D.S.: Two-phase modeling of deflagration-to-detonation transition in granular materials: Reduced equations **3002**(2001) (2001). DOI 10.1063/1.1398042
9. Le Métayer, O., Massoni, J., Saurel, R.: Elaboration des Lois d'Etat d'un Liquide et de sa Vapeur pour les Modeles d'Ecoulements Diphasiques. International Journal of Thermal Sciences **43**(3), 265–276 (2004). DOI 10.1016/j.ijthermalsci.2003.09.002
10. Matheis, J., Hickel, S.: Multi-component vapor-liquid equilibrium model for LES and application to ECN Spray A. Proceedings of the CTR Summer Program, Center for Turbulence Research, Stanford University (2016)
11. Moureau, V., Lartigue, G., Sommerer, Y., Angelberger, C., Colin, O., Poinsot, T.: Numerical methods for unsteady compressible multi-component reacting flows on fixed and moving grids. J. Comput. Phys. **202**(2), 710–736 (2005). DOI 10.1016/j.jcp.2004.08.003. URL http://dx.doi.org/10.1016/j.jcp.2004.08.003
12. Murrone, A., Guillard, H.: A five equation reduced model for compressible two phase flow problems. Journal of Computational Physics **202**(2), 664–698 (2005). DOI 10.1016/j.jcp.2004.07.019
13. Müller, H., Niedermeier, C.A., Matheis, J., Pfitzner, M., Hickel, S.: Large-eddy simulation of nitrogen injection at trans- and supercritical conditions. Physics of Fluids **28**(1), 015,102 (2016). DOI 10.1063/1.4937948. URL http://dx.doi.org/10.1063/1.4937948
14. Oefelein, J.C.: Mixing and combustion of cryogenic oxygen-hydrogen shear-coaxial jet flames at supercritical pressure. Combustion Science and Technology **178**(1-3), 229–252 (2006). DOI 10.1080/00102200500325322. URL http://dx.doi.org/10.1080/00102200500325322
15. Osher, S.J.: Fronts Propagating with Curvature Dependent Speed. Computational Physics **79**(1), 1–5 (1988). DOI 10.1007/s13398-014-0173-7.2
16. Peng, D.Y., Robinson, D.B.: A new two-constant equation of state. Industrial & Engineering Chemistry Fundamentals **15**(1), 59–64 (1976)
17. Perigaud, G., Saurel, R.: A compressible flow model with capillary effects **209**, 139–178 (2005). DOI 10.1016/j.jcp.2005.03.018
18. Poinsot, T.J., Lele, S.K.: Boundary conditions for direct simulations of compressible viscous flows. Journal of Computational Physics **101**, 104–129 (1992). DOI 10.1016/0021-9991(92)90046-2
19. Poling, B.E., Prausnitz, J.M.: the Properties of Gases and Liquids, vol. 123 (2001). DOI 10.1021/ja0048634. URL http://pubs.acs.org/doi/abs/10.1021/ja0048634
20. Richard Saurel, Petitpas, F., Berry, R.A.: Simple and efficient relaxation methods for interfaces separating compressible fluids, cavitating flows and shocks in multiphase mixtures. Journal of Computational Physics **228**(5), 1678–1712 (2009). DOI 10.1016/j.jcp.2008.11.002. URL http://dx.doi.org/10.1016/j.jcp.2008.11.002
21. Schmitt, T.: Simulation des Grandes Echelles de la combustion turbulente à pression supercritique. Institut National Polytechnique de Toulouse (Ph.D Thesis) (2009)
22. Schmitt, T., Méry, Y., Boileau, M., Candel, S.: Large-Eddy Simulation of oxygen/methane flames under transcritical conditions. Proceedings of the Combustion Institute **33**(1), 1383–1390 (2011). DOI 10.1016/j.proci.2010.07.036
23. Schmitt, T., Selle, L.: Large-Eddy Simulation of Supercritical-Pressure Round Jets **48**(9) (2010). DOI 10.2514/1.J050288
24. Soave, G.: Equilibrium constants from a modified redlich-kwong equation of state. Chemical Engineering Science **27**(6), 1197 – 1203 (1972). DOI http://dx.doi.org/10.1016/0009-2509(72)80096-4. URL http://www.sciencedirect.com/science/article/pii/0009250972800964
25. Urbano, A., Douasbin, Q., Selle, L., Staffelbach, G., Cuenot, B., Schmitt, T., Ducruix, S., Candel, S.: Study of flame response to transverse acoustic modes from the les of a 42-injector rocket engine. Proceedings of the Combustion Institute **36**(2), 2633–2639 (2017). DOI 10.1016/j.proci.2016.06.042. URL http://dx.doi.org/10.1016/j.proci.2016.06.042
26. Urbano, A., Selle, L., Staffelbach, G., Cuenot, B., Schmitt, T., Ducruix, S., Candel, S.: Exploration of combustion instability triggering using Large Eddy Simulation of a multiple injector Liquid Rocket Engine. Combustion and Flame **169**, pp. 129–140 (2016). DOI 10.1016/j.combustflame.2016.03.020. URL https://hal.archives-ouvertes.fr/hal-01320509
27. van der Waals, J.D.: The thermodynamic theory of capillarity under the hypothesis of a continuous variation of density. Journal of Statistical Physics **20**, 200–244 (1979). DOI 10.1007/BF01011514
28. Yang, V.: Modeling of supercritical vaporization, mixing, and combustion processes in liquid-fueled propulsion systems. Proceedings of the Combustion Institute **28**(1), 925–942 (2000). DOI http://dx.doi.org/10.1016/S0082-0784(00)80299-4. URL http://www.sciencedirect.com/science/article/pii/S0082078400802994{%}5Cnhttp://ac.els-cdn.com/S0082078400802994/1-s2.0-S0082078400802994-main.pdf?{_}tid=6d88ac7a-396e-11e4-ad9e-00000aacb35e{&}acdnat=1410410897{_}4dc0b5737ebde0cac2fe2beead1070f4